SARS-CoV-2 entry inhibitors by dual targeting TMPRSS2 and ACE2: An *in silico* drug repurposing study

Krishnaprasad Baby [a], Swastika Maity [a], Chetan H. Mehta [b], Akhil Suresh [b], Usha Y. Nayak [b,c], Yogendra Nayak [a,*]

[a] *Department of Pharmacology, Manipal College of Pharmaceutical Sciences, Manipal Academy of Higher Education, Manipal, Karnataka, 576104, India*
[b] *Department of Pharmaceutics, Manipal College of Pharmaceutical Sciences, Manipal Academy of Higher Education, Manipal, Karnataka, 576104, India*
[c] *Manipal McGill Centre for Infectious Diseases, Prasanna School of Public Health, Manipal Academy of Higher Education, Manipal, Karnataka, 576104, India*

ARTICLE INFO

ABSTRACT

The coronavirus disease (COVID-19) is spreading between human populations mainly through nasal droplets. Currently, the vaccines have great hope, but it takes years for testing its efficacy in human. As there is no specific drug treatment available for COVID-19 pandemic, we explored *in silico* repurposing of drugs with dual inhibition properties by targeting transmembrane serine protease 2 (TMPRSS2) and human angiotensin-converting enzyme 2 (ACE2) from FDA-approved drugs. The TMPRSS2 and ACE2 dual inhibitors in COVID-19 would be a novel antiviral class of drugs called "entry inhibitors." For this purpose, approximately 2800 US-FDA approved drugs were docked using a virtual docking tool with the targets TMPRSS2 and ACE2. The best-fit drugs were selected as per docking scores and visual outcomes. Later on, drugs were selected on the basis of molecular dynamics simulations. The drugs alvimopan, arbekacin, dequalinum, fleroxacin, lopinavir, and valrubicin were shortlisted by visual analysis and molecular dynamics simulations. Among these, lopinavir and valrubicin were found to be superior in terms of dual inhibition. Thus, lopinavir and valrubicin have the potential of dual-target inhibition whereby preventing SARS-CoV-2 entry to the host. For repurposing of these drugs, further screening *in vitro* and *in vivo* would help in exploring clinically.

1. Introduction

Coronaviruses, once regarded as relatively innocuous respiratory pathogens in human beings. The previously reported two instances of respiratory tract infections, SARS, and MERS are both zoonotic diseases. SARS-coronavirus (SARS-CoV) was initially found in civets in markets and majorly transmitted through bats. MERS coronavirus typically spreads from camels to humans. SARS-CoV-2 erupted in Wuhan, China, and became a worldwide pandemic COVID-19 (Ye et al., 2020). The frequent indications of COVID-19 are varying degrees of fever, dry cough, headache, anosmia and dysgeusia, sore throat, and diarrhoea. Usually, death is due to comorbidity such as diabetes, hypertension, renal and liver disorders, asthma etc. (Lovato and de Filippis, 2020). The inflammatory response in alveoli of the lung makes it difficult for gas exchange. It is now evident that the death in COVID-19 is because of the acute release of inflammatory mediators and "cytokine storm" (Coperchini et al., 2020). Hence, immunomodulators such as dexamethasone and prednisolone were approved by regulatory agencies across the world. The SARS-CoV-2 generally spreads by nasal droplets. Hence social distancing, isolation, and quarantine are the best-suggested methods for preventing the disease (Chu et al., 2020). Currently, prevention of infection, and supportive treatments such as oxygen therapy and mechanical ventilation, are the strategies for managing COVID-19 till the specific treatment is established (Sanders et al., 2020). Vaccines are currently under trial, and the efficacy of convalescent plasma is limited. The approved specific antiviral agents such as remdesivir and favipiravir do not produce a complete cure (Lu et al., 2020). Hence, the fast-tracking of drug discovery and development is inevitable. Many scientists have proposed drug repurposing. In drug-repurposing, the *in silico* screening offers an excellent and rapid drug screening (Deshpande et al., 2020).

We have used computational tools to study the drug-targeting "main

---

protease" (M[pro]) and "RNA-dependent RNA polymerase" (RdRp) for the repurposing of US-FDA-approved drugs (Baby et al., 2020a, 2020b, 2021). The crucial step in computational drug repurposing is the selection of validated drug-target. We envisaged that inhibiting the host cell entry would prevent viral load. The access of coronavirus into the host cell is enabled by two main drug targets, "human angiotensin-converting enzyme 2" (ACE2) and transmembrane serine protease 2 (TMPRSS2) (Hoffmann et al., 2020). Hence we selected these two targets for our studies. The SARS-CoV-2 spike protein (S) attaches to ACE2 with 10–20 folds higher affinity than the SARS-CoV spike glycoprotein. It might contribute to the spread of COVID-19 from humans to humans at high-speed (Wrapp et al., 2020). The TMPRSS2, a host-cell serine-protease enzyme, and ACE2 facilitate endocytosis and endosome-containing coronavirus (Hou et al., 2020). The dual-targeting, as a viral entry inhibitor, is a novel approach for anti-SARS-CoV-2 treatment. Hence, in this study, we examined FDA approved drugs for inhibiting serine protease TMPRSS2 and human ACE2. We prepared the protein backbone of the TMPRSS2 enzyme by homology modelling and used ACE2 for docking and molecular dynamics simulations.

2. Materials and methods

2.1. Computational simulation

The *in silico* modelling, screening, and simulation experiments were executed on Ubuntu desktop workstation, on the Maestro graphical user interface of Schrödinger Suite (www.schrodinger.com) in an Intel® Xenon® Gold 6130 CPU @ 2.10 GHz x 64 processors, Quadro P620/PCle/SSE2 graphics card, and 8 GB RAM.

2.2. TMPRSS2 homology modelling and protein preparation

There was no available and curated crystal structure for TMPRSS2 in the PDB database. Hence, the amino acid sequence of the catalytic domain of TMPRSS2 protein was imported from www.uniprot.org with the code of UniProtKB-O15393 (Boutet et al., 2016). BLAST Homology search tool was employed to look for an acceptable prototype to create a homology TMPRSS2 model. The homology model was created using the human plasma kallikrein (PDB ID: 5TJX) model as a reference utilising Schrodinger Prime Module (Jacobson et al., 2004; Vyas et al., 2012). The modelled structure was later modified by Refine Loops software. Thus the optimised homology model was validated by the "Ramachandran plot" (Ramachandran et al., 1963). Based on the resolution, the best TMPRSS2 homology model was later used in molecular docking experiments. The protein TMPRSS2 was created by homology-modelling and was further optimised (Madhavi Sastry et al., 2013). A proper ionisation status was defined at pH 7.4 through PROPKA3 (Olsson et al., 2011; Rostkowski et al., 2011). The protein structure was then minimised using the restricted minimisation technique.

2.3. ACE2 protein preparation

The X-ray diffraction crystallographic human ACE2 associated inhibitor carboxypeptidase protein structure (PDB ID: 1R4L) was acquired from PDB (www.rcsb.com) with a resolution of 3.00 Å (Madhavi Sastry et al., 2013). The Protein Prep Wizard (PPW) was used to refine and optimise the protein structure. The Prime tool in Schrodinger was applied for adding the missing hydrogen bonds, side chains, and missing residues. The bulky water molecules were removed (Olsson et al., 2011; Rostkowski et al., 2011). The active site and essential catalytic residues were preserved in the protein structure.

2.4. Ligand preparation

The chemical structure of compounds licensed by USFDA (~2800

Nos) was saved from www.drugbank.ca. Proper ligand alignments were produced on the molecules, wherein they formed 3D coordinates. (Chen and Foloppe, 2010). The accurate degree of ionisation was assessed at pH 8.0. Through LigPrep, 2-dimensional chemical structures were converted to 3-dimensional structures with multiple configurations of each input chemical structure with diverse ionisation states, tautomers, stereochemistries, ring conformations. The resulting structures were then saved in Maestro format (Shelley et al., 2007). Finally, the moiety was converted into a lower energy level by lowering energy using the OPLS3e force field (Roos et al., 2019). The Ligand structures so prepared by LigPrep were then used for docking studies.

2.5. Ligand docking

The docking was executed utilising the Glide Module in Schrodinger suit. The linking position of molecular ligands was analysed based on the bound ligand and its centroid identified by the Glide grid tool (Friesner et al., 2004). The co-crystalline ligand was separated during ligand docking. Initially, ~2800 FDA-acquiesced molecules were docked independently into the receptor grids developed on TMPRSS2 and ACE2 using Schrodinger's High Throughput Virtual Screening (HTVS) (Damm-Ganamet et al., 2019). Later, the Standard Precision (SP) docking technique was used on top molecules, high docking scores. Also, their protein-ligand interaction contacts were analysed independently against both targets. Afterwards, based on the SP docking score, ligand-protein contacts and visual analysis of specific molecules were examined, and the molecules were chosen for further analyses.

2.6. Molecular dynamics (MD) simulation

This study was performed using the Schrodinger Desmond platform, and it helps assess patterns of interaction among proteins and ligands and time-dependent protein-ligand interaction associations and conformational dynamics of complex systems. The predicted structures of human ACE2 and TMPRSS2 combined with ligands observed during Glide SP docking were used in MD simulations as explained in our previous work (Baby et al., 2020b).

## 3. Results

3.1. TMPRSS2 homology and ACE2

The TMPRSS2 homology model was found suitable for the docking studies when it was validated by the Ramachandran plot (Fig. 1). Further, human ACE2 protein preparation was found to be suitable for docking studies.

3.2. Results of ligand docking

Original ligand docking of ~2800 FDA approved drugs were performed separately to recognise how they bind to host proteins TMPRSS2 and ACE2. The ligand docking offered ample knowledge of the affinity and orientation of ligand-protein complexes which impairs the protein activity. Initially, ~2800 molecules were subjected to HTVS separately on both the targets. Then top drugs obtained on HTVS (top-500) based on the docking scores were further docked under Standard Precision (SP) docking. All the top-500 molecules were observed by visual examination for intermolecular interactions. The specific drugs, those interacted strongly with the TMPRSS2 homology model, and ACE2 were identified and shortlisted. Tables 1 and 2 represents intramolecular interactions in SP-docking with TMPRSS2 and ACE2, respectively.

3.3. Binding mode of shortlisted drugs

The frequent hits against target TMPRSS2 and ACE2 were identified upon visual examination. The drugs such as valrubicin, lopinavir,
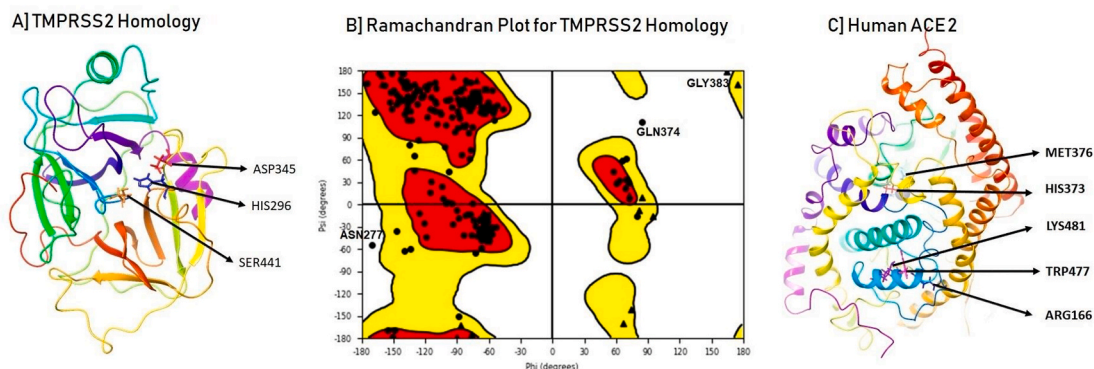
Fig. 1. Protein structures and Ramachandran plot.
A) Homology model of TMPRSS2 showing catalytic sites, because the TMPRSS2 crystal structure was not available in PDB, the sequence was obtained from UniProtKB-O15393 and the homology model was created using the human plasma kallikrein PDB ID-5TJX; B) Ramachandran plot for optimised homology model of TMPRSS2, here the number of outliers in homology generated molecule of TMPRSS2 is less, which proves that the developed homology model is fit for further studies; C) ACE2 with catalytic site (PDB ID: 1R4L); th figure are obtained from the Maestro graphical user interface of Schrödinger Suite.

Table 1
Intermolecular interactions of shortlisted drugs against TMPRSS2.

| Sl No	Name of Molecule	Docking Score	π-π interactions	π-cation interactions	Hydrogen bonding interactions	Salt bridges	Hydrophobic Interactions
1	Valrubicin	−7.188	TRP461	-	-	LYS300, LY439, TRP461	CYS281, VAL280, CYS465, CYS437
2	Lopinavir	−7.261	-	LYS340	LYS300, LYS340	GLU299, TRP461	CYS437, CYS465,
3	Fleroxacin	−7.096	HIS296, TRP461	TRP461	-	LYS300	TYR337, LEU419, ILE420, MET424, TRP461
4	Alvimopan	−7.902	TRP461	HIS296	-	LYS300	TYR337, CYS437, TRP461, CYS465
5	Arbekacin	−7.232	-	TRP461	GLU299, LYS300, LYS340, ASP345, ASP435	GLU299, ASP435	TYR337, CYS437, TRP461, CYS465, ALA466
6	Dequalinium	−8.397	TRP461	TRP461	GLY464	-	LEU419, ILE420, MET424, CYS437, TRP461, CYS465, VAL473

Table 2
Intermolecular interactions of shortlisted drugs against ACE2.

Sl No	Name of Molecule	Docking Score	Metal Coordination	π-π interactions	π-cation interactions	Hydrogen bonding interactions	Salt bridges	Hydrophobic Interactions
1	Valrubicin	−8.594	-	-	ARG273, ARG518	ASN149, LYS363	-	TYR127, MET152, ALA153, TRP168, PHE274, TRP271, MET270, LEU370, LEU143, LEU144, VAL343, CYS344, PRO346, PHE504
2	Lopinavir	−7.890	-	PHE274	-	ASH368, ARG273 LYS363, THR371	-	TYR127, LEU144, ALA153, PHE214, TRP271, CYS344, PRO346, CYS361, MET366, LEU370 TYR515
3	Fleroxacin	−7.739	-	HIS374	ARG518	ARG273, ASP367 HIE345	ASP367	ALA153, PHE274, TYR515
4	Alvimopan	−8.516	ZN803	-	LYS363	ARG273, ASN277 ASP367, THR371	ZN803	ALA153, MET270, TRP271, PHE274, PRO346, MET360, LEU370, TYR515
5	Arbekacin	−7.748	ZN803	-	PHE274	ASP367, ARG273 PRO346, CYS361 THR371, GLU375	GLU145, ASP367, GLU375	ALA153, TRP271, PHE274, PRO346, ALA348, MET360, CYS361, LEU370, TYR515
6	Dequalinium	−7.738	-	HIE345	HIE345	ALA348, ASH368	-	PHE274, CYS344, PRO346, ALA348, TRP349, MET360, CYS361, PHE504, TYR510, TYR515

fleroxacin, alvimopan, arbekacin, and dequalinium exhibited a compelling binding mode against both the targets. Fig. 2 represents the structures of the shortlisted molecules. These molecules interacted with the various residues of protein through H-bond, Salt-bridge, π-π interaction, and π-cation interaction with TMPRSS2 and ACE2. Figs. 3 and 4 depict valrubicin and lopinavir bound against TMPRSS2 and ACE2 as superior to other ligands.

3.4. Results of MD-simulation

The molecular dynamics (MD) simulation investigation established structural insights into the protein-ligand complex's molecular interaction based on observed variations in root mean square deviation (RMSD) and their stability under simulated physiological conditions using the Maestro Desmond module. MD simulation was performed on the ligands that demonstrated stronger ligand-protein interactions, namely valrubicin, lopinavir, fleroxacin, alvimopan, arbekacin, and dequalinium following SP-docking. Examination of RMSD variations demonstrated
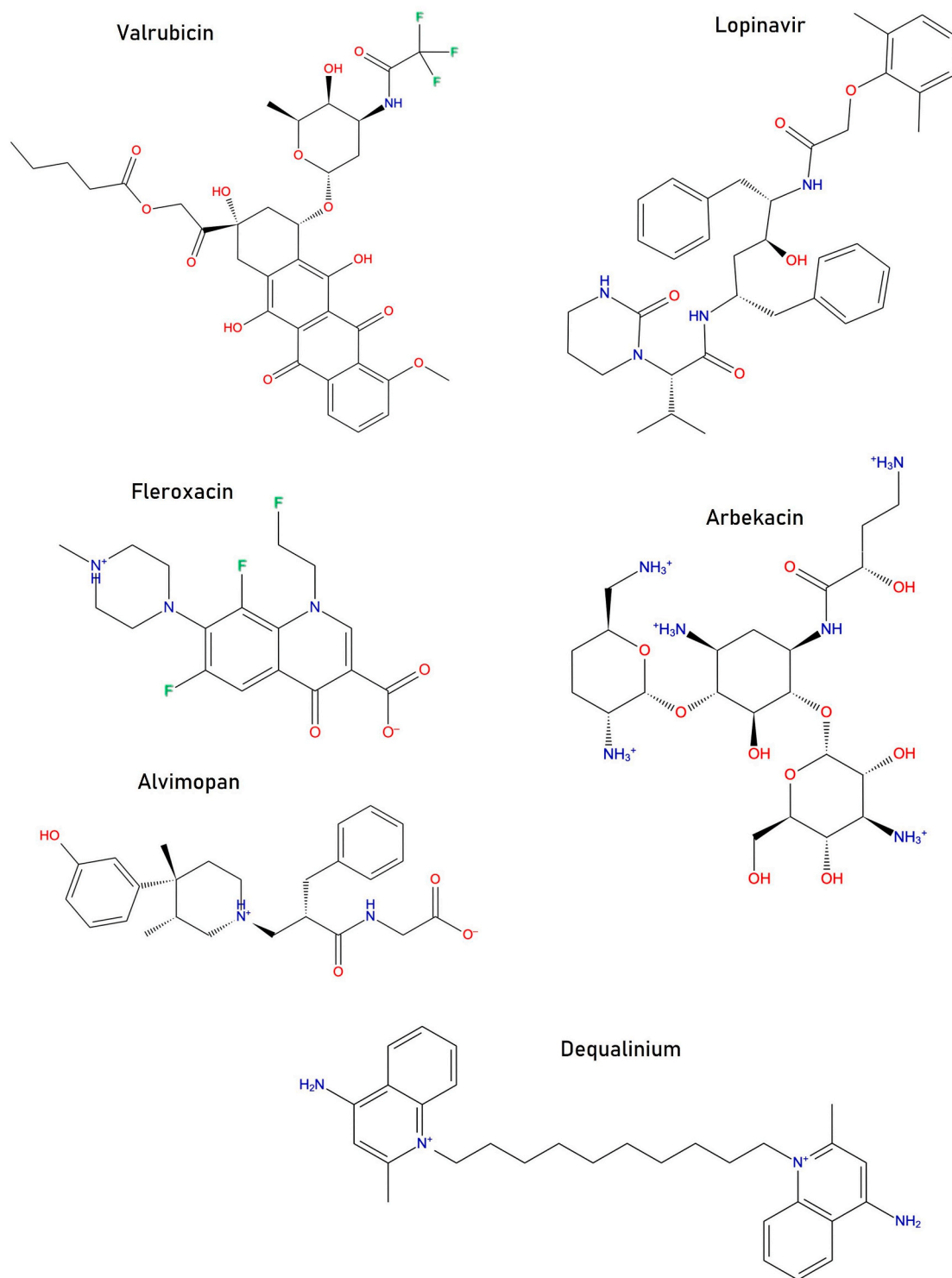
Fig. 2. Chemical structures of drugs shortlisted as SARS-CoV-2 entry inhibitors.
These drugs have displayed good binding on TMPRSS2 and ACE2 upon standard precision (SP)-docking. Further, the interaction was confirmed by MD simulations.

that valrubicin and lopinavir displayed binding with the targets while the ligand and protein RMSD oscillations stayed within 2.0 Å. Figs. 5 and 6 show the ligand and protein RMSD plot while simulating ligand-protein complexes during MD simulations.

The TMPRSS2 bound with valrubicin complex displayed hydrophobic and hydrophilic interactions during MD simulations. The narrative of the protein structure backbone specified during the MD simulations was compared with the original structure for the RMSD analysis. After initial

variations due to equilibration for 50 nsec, the RMSD for protein structures was maintained from 0.40 to 4.2 Å until the simulation. (Fig. 5). It was observed that the fluctuations for protein have remained within 0.20 Å, which indicated a highly stable protein structure. Similarly, the fluctuations remained within 1.5 Å, which indicated a highly stable ligand in the protein complex. Fig. 7 illustrates the ligand-protein interactions recorded during the MD simulation. The amino acid residue TRP461 made maximum contact with the ligand throughout
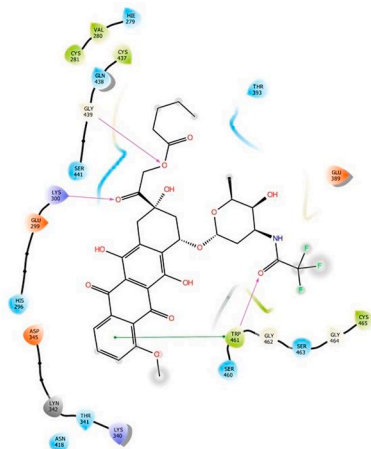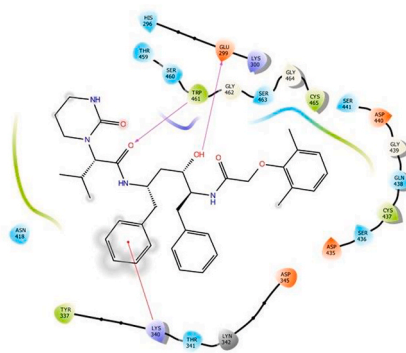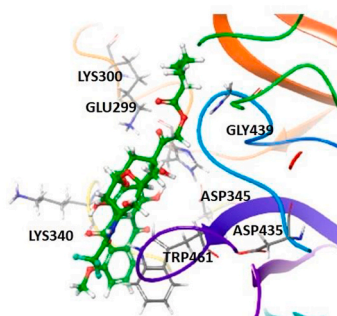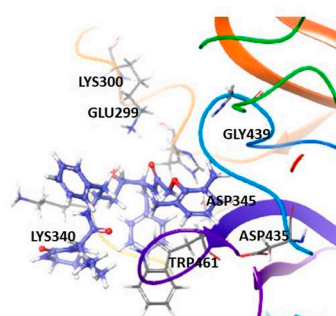
Fig. 3. 2D and 3D interactions of valrubicin and lopinavir with TMPRSS2.
Ligand interaction with the target TMPRSS2; different bonding with important amino acid residues are shown. These interactions are further explained in Table 1. Figures are obtained from Maestro graphical user interface of Schrödinger Suite.

simulations. In the simulation, bridged hydrogen bonding, π-cation interactions, and direct hydrogen bonding with protein's residues were observed. The residue TRP461 interacted with the ligand via a π-π stacking, which accounted for 30 and 40% of the interactions.

The valrubicin-bound ACE2 illustrated hydrophilic interactions during the MD simulations. A plot of protein backbone structure described during the MD simulations were compared to the original structures for the RMSD. After initial variations due to balancing, for a period of 50 nsec, until the end of the simulation, the RMSD for protein structures was held between 0.30 and 1.8 Å (Fig. 6). The protein fluctuations that persisted within 0.30 Å proved a stable protein structure. Fluctuations for the ligand was persisted within 2.1 Å, suggesting a stable ligand in the protein complex. Fig. 8 displays the ligand-protein contacts identified during the MD simulation. The residue ASN149 made full interaction with valrubicin during the simulations. Bridged hydrogen bonding with different amino acid residues, namely GLU145, ASN149, ASP367, THR371, were observed during the simulation.

TMPRSS2 bound to the lopinavir complex demonstrated mainly hydrophilic associations during molecular simulations. The plot of the protein structure of the backbone listed during the MD simulations matched with the initial structure of the RMSD. After preliminary variations due to equilibration, for initial 50 nsec, the RMSD for protein structure stayed between 1.4 and 2.8 Å till the completion of simulations (Fig. 5). The fluctuations that persisted within 0.8 Å showed a stable protein structure. The variations persisted within 7.6 Å, suggesting a relatively unstable ligand within the protein complex. Fig. 9 depicts the ligand-protein contacts and the protein-ligand contacts recorded during the MD simulations. The TRP461 and LYS300 residues made full interaction with the lopinavir. A direct hydrogen bonding was demonstrated

with amino acid residue TRP461 and the unsaturated double-bonded ligand oxygen, which accounted for 70% of the interactions. Further, the bridged hydrogen bonding with HIS296, LYS300, GLY439, and GLY462 formed by 30, 77, 34, and 39% of the interactions were observed. Similarly, a direct hydrogen bond was formed, which forms 70% of the interactions. Many of the associations found amongst protein and ligand throughout docking was reliably maintained during MD simulation.

The protein ACE2 linked to the lopinavir complex demonstrated mostly hydrophilic interactions during MD simulation. The plot of the target protein backbone described during MD simulations were compared with the original structure for the RMSD analysis. After preliminary variations due to equilibration, for a duration of 50 nsec, the RMSD between 0.25 and 1.75 Å until the end of the simulation Fig. 6. The fluctuations for the protein that persisted within 0.25 Å suggested a highly stable protein structure. The fluctuations remained within 1.8 Å, indicating a highly unstable ligand in the protein complex. Fig. 10 depicts the ligand-protein contacts and the protein-ligand contacts recorded during the MD simulation. The residue ARG273 made maximum contact with the ligand throughout simulations. Bridged H-bonding, π-cation interactions, and direct hydrogen bonding with protein residues were observed in the simulation. The residue ARG273 interacted with the ligand via a π-cation and two direct hydrogen bonds, which accounted for 52, 68, and 79%, respectively.

Similarly, bridged hydrogen bonding was with ASP367 and GLU406, which accounted for 62 and 46%, respectively. These results suggest that drugs like valrubicin and lopinavir have superior binding among shortlisted drugs. Further, the other drugs such as fleroxacin, arbekacin, alvimopan, and dequalinium were also identified as useful dual
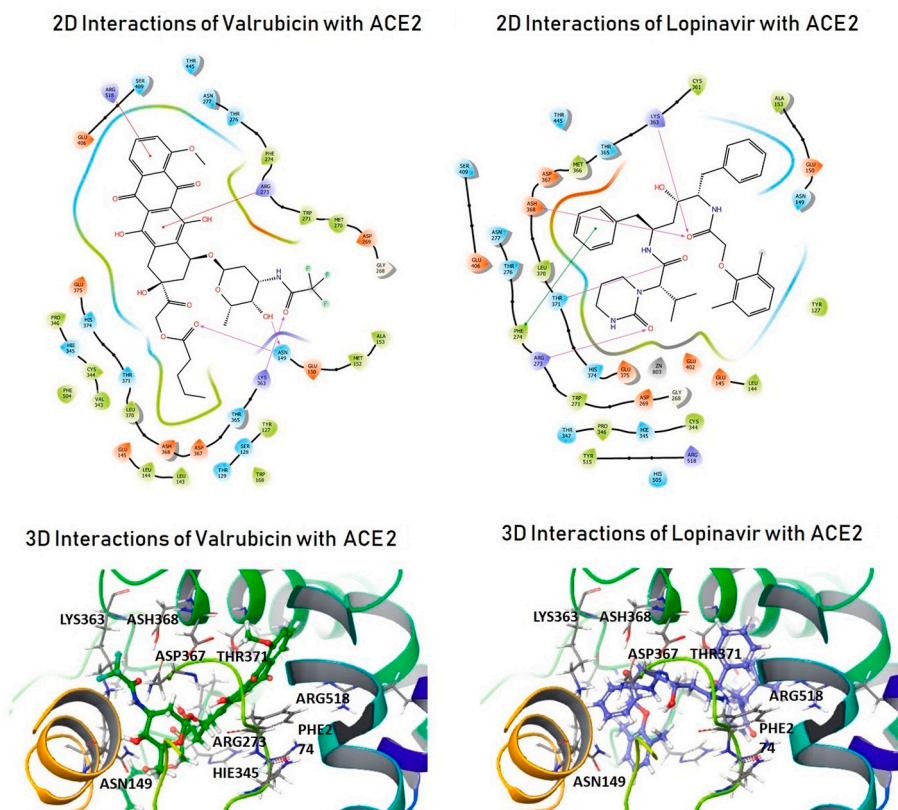
Fig. 4. 2D and 3D interactions of valrubicin and lopinavir with human ACE2.
Ligand interaction with the target ACE2; different bonding with important amino acid residues are shown. These interactions are further explained in Table 2.
Figures are obtained from Maestro graphical user interface of Schrödinger Suite.
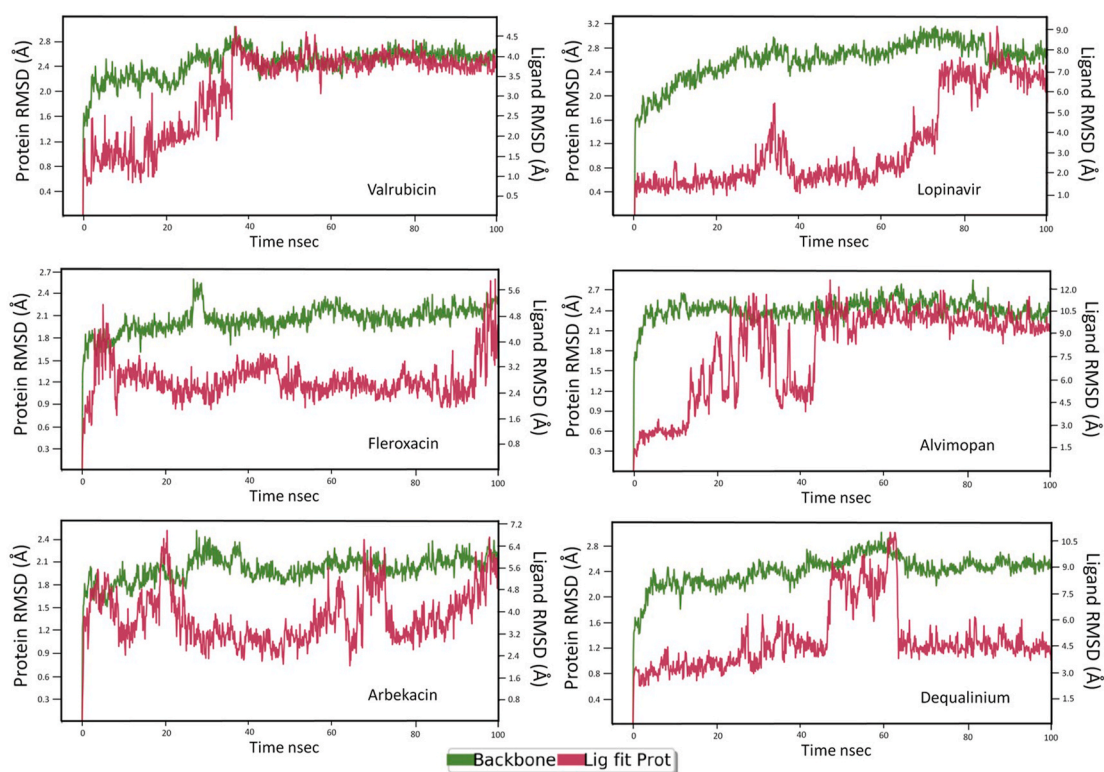
Fig. 5. Route mean square deviations (RMSD) plots of TMPRSS2 protein-ligand interactions of shortlisted drugs; The MD simulation was run for 100 nsec; The green colour represents the backbone protein RMSD, and violet coloured graph represents the ligand RMSD. The ligand-protein interaction is highly stable if the fluctuations are not more than 1.5 Å.
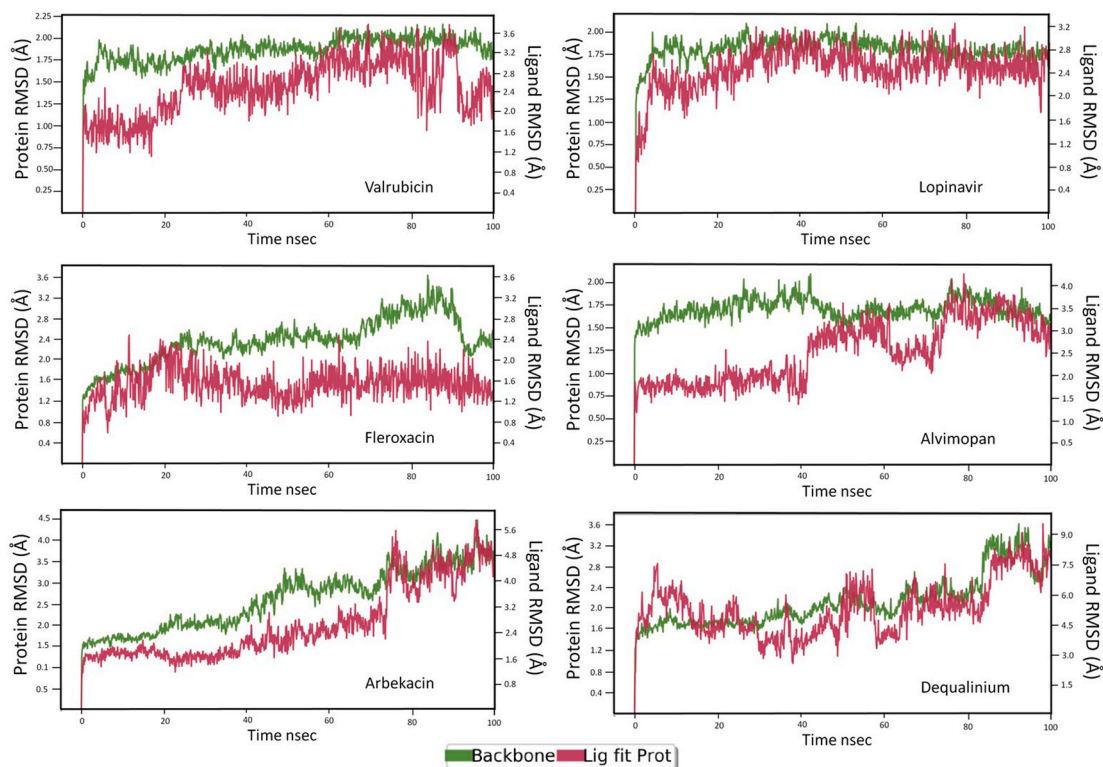
Fig. 6. Route mean square deviations (RMSD) plot of human ACE2 protein-ligand interactions of shortlisted drugs; The MD simulation was run for 100 nsec; The green colour represents the backbone protein RMSD, and violet coloured graph represents the ligand RMSD. The ligand-protein interaction is highly stable if the fluctuations are not more than 1.5 Å.
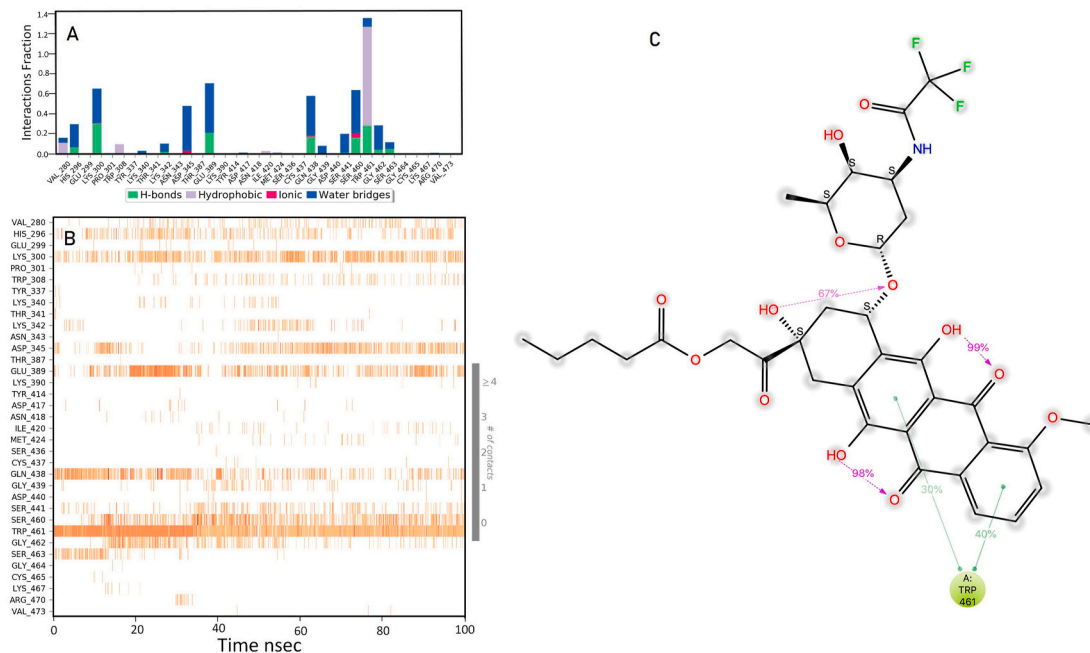
Fig. 7. Interaction diagram of valrubicin with TMPRSS2 obtained during MD simulations.
A: The protein-ligand interaction diagram. B: Amino acid residues that interact with the ligand in each trajectory frame. The residues making strong contacts are shown in darker colour shade. C: Ligand interaction with the amino acid residues of protein during MD simulation. Interactions that occur more than 30% of the simulation time are shown.

inhibitors by SP-docking, binding orientation, and interaction patterns. These ligands, whose molecular interaction pattern is represented in the supplementary files (Figs. S1–S8).

4. Discussion

Evolutionarily, SARS-CoV-2 comprises four major structural proteins, namely spike (S), envelope (E), membrane (M), and nucleocapsid

Fig. 8. Interaction diagram of valrubicin with ACE2 obtained during MD simulations.
A: The protein-ligand interaction diagram. B: Amino acid residues that interact with the ligand in each trajectory frame. The residues making strong contacts are shown in darker colour shade. C: Ligand interaction with the amino acid residues of protein during MD simulation. Interactions that occur more than 30% of the simulation time are shown.
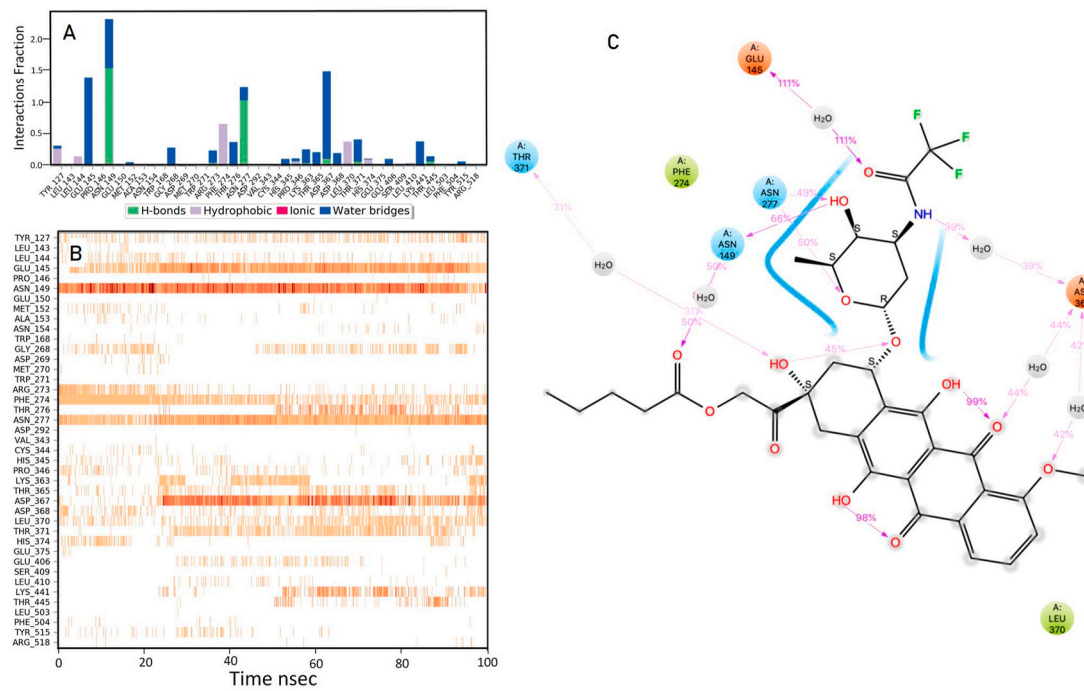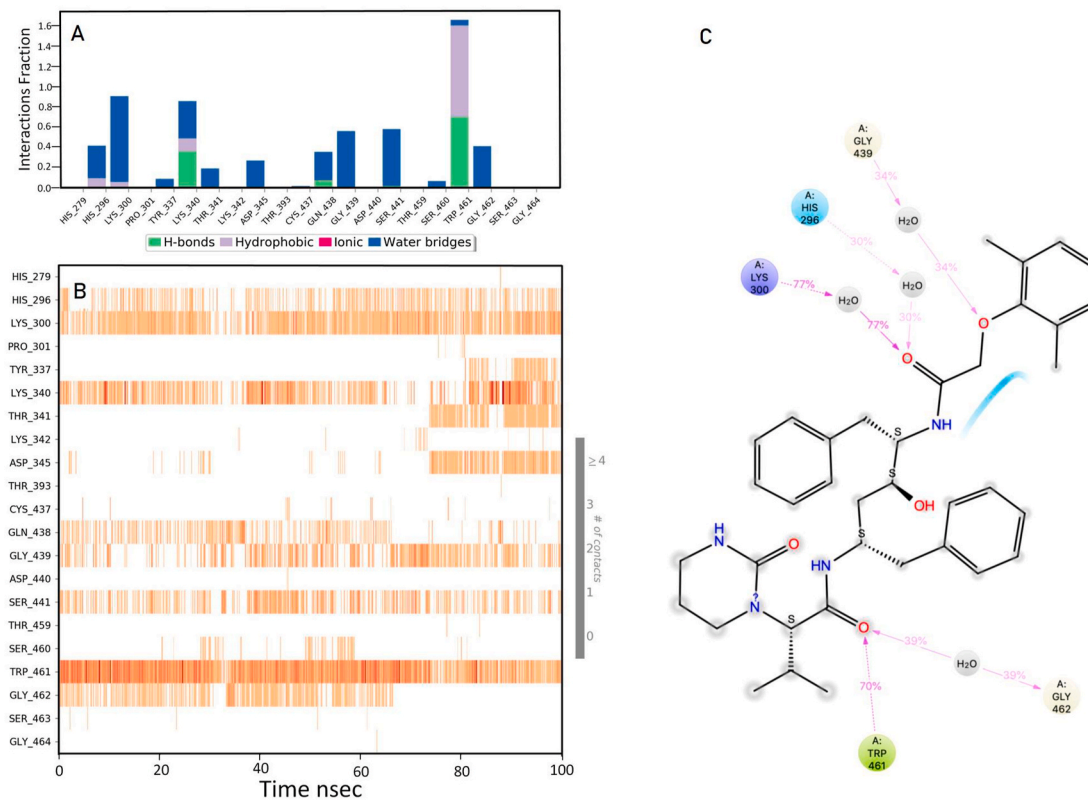

Fig. 9. Interaction diagram of lopinavir with TMPRSS2 during MD simulations.
A: The protein-ligand interaction diagram. B: Amino acid residues that interact with the ligand in each trajectory frame. The residues making strong contacts are shown in darker colour shade. C: Ligand interaction with the amino acid residues of protein during MD simulation. Interactions that occur more than 30% of the simulation time are shown.

Fig. 10. Interaction diagram of lopinavir with ACE2 during MD simulations.
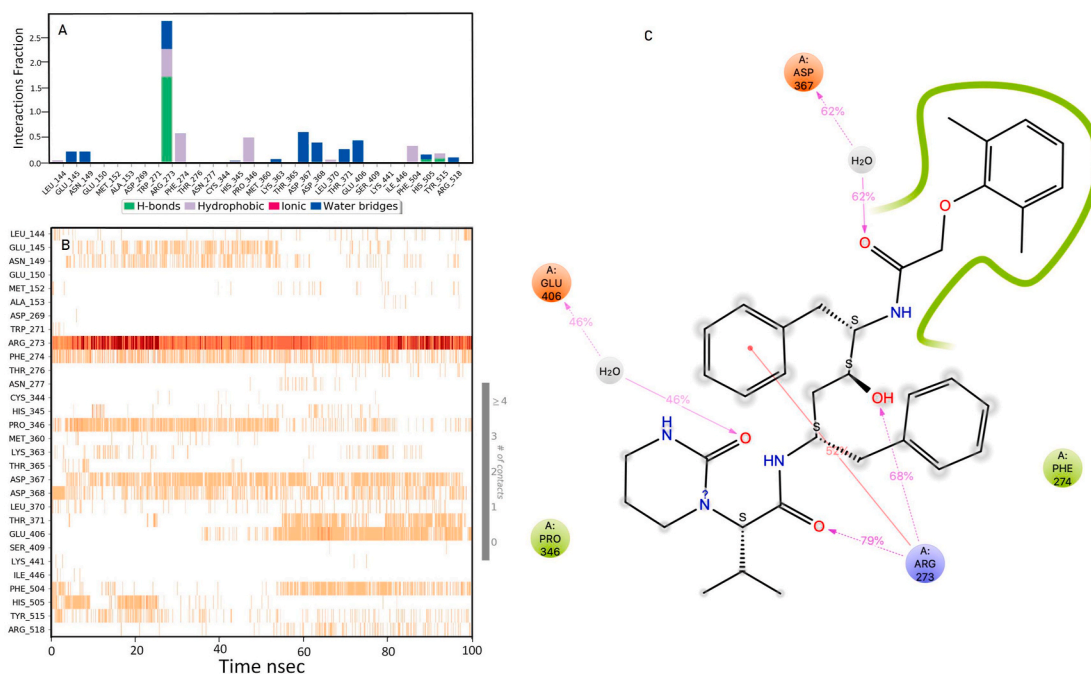A: The protein-ligand interaction diagram. B: Amino acid residues that interact with the ligand in each trajectory frame. The residues making strong contacts are shown in darker colour shade. C: Ligand interaction with the amino acid residues of protein during MD simulation. Interactions that occur more than 30% of the simulation time are shown.

(N) protein, together with many accessory proteins (Jiang et al., 2020). The S-protein is a transmembrane protein in the outer part of the virus, with a molecular weight of around 150 kDa (Walls et al., 2020). Infection with SARS-CoV-2 relies on human ACE2 for entry into the cell and TMPRSS2 (Hoffmann et al., 2020). SARS-CoV-2 primarily infects the pneumocytes and macrophages of the lungs. The S-protein is cleaved and activated by TMPRSS2, before membrane fusion. This makes the transfer of viral contents into the cytoplasm of the pneumocytes (Hoffmann et al., 2020). ACE2 has been shown to transform angiotensin-2 into angiotensin 1–7, which attaches to the Mas-receptor to counteract the angiotensin 2 receptor leading to vasoconstriction and pro-inflammatory effects (Simões E Silva et al., 2013). Angiotensin 2 moderates its effects by activating MAPK at p38 (Park et al., 2007). Angiotensin 1–7 Mas-receptor stimulation reduces p38 MAPK activation to ameliorate inflammation (Yu et al., 2018). Therefore, blocking ACE2 after coronavirus entry might cause Angiotensin 2 induced p38 activation to dominate in heart and lungs because of Angiotensin 1–7 down-regulation. This in turn, stimulates the inflammatory process and creates a positive feedback loop due to p38 mediated upregulation of ADAM17, a protease which severs the ACE2 ectodomain to further the defensive function of local ACE2 (Zipeto et al., 2020). In the present computational investigation, we observed six molecules, namely alvimopan, arbekacin, dequalinium, fleroxacin, lopinavir, and valrubicin, as a potent inhibitor of both TMPRSS2 and ACE2 by docking and MD-simulations. These shortlisted drugs will be helpful in mitigating the inflammatory processes associated with TMPRSS2 and ACE2. The usage of these established drugs to SARS-CoV-2 might render them superior over other currently used drugs. The MD simulations indicated the association of valrubicin and lopinavir against TMPRSS2 and human ACE2 demonstrated stronger binding stability. The RMSDs of valrubicin and lopinavir complexes with both the proteins TMPRSS2 and ACE2 were stable than other shortlisted drugs. Moreover, both the ligands exhibited an excellent binding interaction with amino acid residues of TMPRSS2 throughout the simulations. The same was observed with valrubicin and lopinavir interactions with the catalytic triad of human ACE2. Hence, we have ranked valrubicin, and lopinavir as best hits against the targets

TMPRSS2 and ACE2.

Alvimopan is a peripheral opioid mu-receptor antagonist for improving postoperative gastrointestinal recovery in patients with ileus and is devoid of severe adverse effects (Xu et al., 2016). The drug arbekacin is efficacious towards gram-positive bacteria, and methicillin-resistant *Staphylococcus aureus*, without any chronic, dangerous, or life-threatening adverse events. It is efficacious when administered as inhalation in patients with pneumonia caused by *P. aeruginosa* and MRSA (Lee and Lee, 2016). Dequalinium chloride is an antimicrobial agent generally used for skin and vagina (Mendling et al., 2016). Advantages of dequalinium is that it also has modulations on inflammation, especially pharyngitis (Cooper et al., 2008). Fleroxacin is a tri-fluorinated quinolone with a broad-spectrum activity, often used in managing intra-abdominal abscesses and of traveller's diarrhoea as well as in pharmacokinetic studies. Fluoroquinolone displayed antimicrobial activity against several infections caused by mycobacteria, mycoplasma, chlamydia, legionellae, etc. (Blouin et al., 1992; Steffen et al., 1993).

We observed a good *in silico* binding of valrubicin and lopinavir among shortlisted drugs could be beneficial in preventing the entry of SARS-CoV-2 and in reducing molecular virulence. Lopinavir was discovered to be a type-1 aspartate protease antagonist of the HIV, which has shown *in vitro* inhibition effect against SARS-CoV-2 (Choy et al., 2020; Kang et al., 2020). The combination of lopinavir-ritonavir was tried for the management of COVID-19 in India, and the reports are not discouraging (clinical trial registry CTRI/2020/06/026196 (http://ctri.nic.in/) (Bhatnagar et al., 2020). Likewise, ritonavir co-administration impair lopinavir metabolism and improve ritonavir plasma levels. The same study reports the possibilities of combining lopinavir-ritonavir with ribavirin in COVID-19 (Zeitlinger et al., 2020). The triple antiviral therapy, lopinavir-ritonavir, and ribavirin with interferon beta-1b was found safe and superior over the lopinavir-ritonavir multicentric, prospective, open-labelled, randomised, phase-2 trial in adults with COVID-19 (Hung et al., 2020). However, Cao et al., 2020 did not see much advantage from treatment with lopinavir/ritonavir relative to normal care in the hospitalised adult with severe Covid-19 symptoms (Cao et al., 2020). Though

lopinavir-ritonavir combination was not successful with standard medical treatment in a randomised, controlled, open-label study in patients with SARS-CoV-2 infection and positive symptoms, Cao et al., 2020 have not entirely rejected the use in the treatment of COVID-19. The subgroup analysis suggests that the lopinavir-ritonavir combination still has efficacy (Cao et al., 2020).

Further, the emergency use of lopinavir-ritonavir combination is accepted in the USA, Japan, Italy, China, and India (Frediansyah et al., 2020). Additionally, valrubicin influences many intracellular physiological functions affecting nucleic acid metabolism, which was earlier found to be a semi-synthetic, anthracycline doxorubicin counterpart could be an alternative drug based on its binding stabilities on dual targets such as ACE2 and TMPRSS2. Wang J., 2020 has reported the bindings to major protease (M^{pro}) by computational studies for *in silico* repurposing in COVID-19 and shortlisted compounds, including lopinavir (Wang, 2020). Our current study found it also has actions as dual inhibition as an entry inhibitor. Thus valrubicin has added advantages if it is tried further for *in vitro* and *in vivo* studies despite its limitations as cardiotoxicity at higher doses (Lotrionte et al., 2013). Hence lopinavir and valrubicin, which might act as potential dual inhibitors of TMPRSS2 and ACE2, could be further studied *in vitro* and *in vivo* models of TMPRSS2 and ACE2 inhibition to confirm the *in silico* predictions.

5. Conclusion

In this study, we provided possible SARS-CoV-2 entry inhibitors through inhibiting TMPRSS2 and ACE2. We conducted virtual screening of commercially available drugs licensed by the FDA, and analysis through MD simulations shortlisted six drugs. Valrubicin and lopinavir were found superior among the drugs shortlisted. Since these drugs have the least degree of toxicity, they may be explicitly tested for their beneficial role in COVID-19 infection followed *in vitro*, *in vivo*, and further clinical investigations.

Funding

Ethics approval

No ethical approval was necessary for these experiments.

Availability of data and material

There are figures supplied as supportive or supplementary files. Other than this, the manuscript has all the data generated by the experiments. But, if any data other than these, authors are ready to supply. Please see the MD simulation data of alvimopan, arbekacin, dequalinium, and fleroxacin as supplementary figures (Figs. S1–S8).

CRediT authorship contribution statement

Krishnaprasad Baby: Conceptualization, Methodology, Formal analysis, Writing - original draft, Writing - review & editing, Writing draft and Editing. **Swastika Maity:** Methodology, Validation, Data curation, Data validation, Visualization, Writing - original draft, Draft writing. **Chetan H. Mehta:** Methodology, Validation, Data validation, Visualization, Data curation, Curating the data. **Akhil Suresh:** Methodology, Data curation, Formal analysis, Data analysis, Visualization. **Usha Y. Nayak:** Conceptualization, Resources, Funding acquisition, Formal analysis. **Yogendra Nayak:** Conceptualization, Formal analysis, Data curation, Curation, Writing - original draft, Writing - review & editing, Writing draft and Editing, Corresponding author.

Declaration of competing interest

"Authors declare that there is no interest in publishing the data generated by this research work".

Appendix A. Supplementary data

Supplementary data to this article can be found online at https://doi.org/10.1016/j.ejphar.2021.173922.

References

Baby, K., Maity, S., Mehta, C., Suresh, A., Nayak, U.Y., Nayak, Y., 2020a. In silico drug repurposing of penicillins to target main protease Mpro of SARS-CoV-2. Pharmaceut. Sci. 26, S52–S62. https://doi.org/10.34172/PS.2020.44.
Baby, K., Maity, S., Mehta, C.H., Suresh, A., Nayak, U.Y., Nayak, Y., 2020b. Targeting SARS-CoV-2 RNA-dependent RNA polymerase: An in silico drug repurposing for COVID-19, 9. F1000Research 9, 1166. https://doi.org/10.12688/f1000research.26359.1.
Baby, K., Maity, S., Mehta, C.H., Suresh, A., Nayak, U.Y., Nayak, Y., 2021. Targeting SARS-CoV-2 main protease: a computational drug repurposing study. Arch. Med. Res. 52, 38–47. https://doi.org/10.1016/j.arcmed.2020.09.013.
Bhatnagar, T., Murhekar, M., Soneja, M., Gupta, N., Giri, S., Wig, N., Gangakhedkar, R., 2020. Lopinavir/ritonavir combination therapy amongst symptomatic coronavirus disease 2019 patients in India: protocol for restricted public health emergency use. Indian J. Med. Res. 151, 184–189. https://doi.org/10.4103/ijmr.IJMR_502_20.
Blouin, R.A., Hamelin, B.A., Smith, D.A., Foster, T.S., John, W.J., Welker, H.A., 1992. Fleroxacin pharmacokinetics in patients with liver cirrhosis. Antimicrob. Agents Chemother. 36, 632–638. https://doi.org/10.1128/AAC.36.3.632.
Boutet, E., Lieberherr, D., Tognolli, M., Schneider, M., Bansal, P., Bridge, A.J., Poux, S., Bougueleret, L., Xenarios, I., 2016. Uniprotkb/swiss-prot, the manually annotated section of the uniprot knowledgebase: how to use the entry view. Methods Mol. Biol. 1374, 23–54. https://doi.org/10.1007/978-1-4939-3167-5_2.
Cao, B., Wang, Y., Wen, D., Liu, W., Wang, Jingli, Fan, G., Ruan, L., Song, B., Cai, Y., Wei, M., Li, X., Xia, J., Chen, N., Xiang, J., Yu, T., Bai, T., Xie, X., Zhang, L., Li, C., Yuan, Y., Chen, H., Li, Huadong, Huang, H., Tu, S., Gong, F., Liu, Y., Wei, Y., Dong, C., Zhou, F., Gu, X., Xu, J., Liu, Z., Zhang, Y., Li, Hui, Shang, L., Wang, K., Li, K., Zhou, X., Dong, X., Qu, Z., Lu, S., Hu, X., Ruan, S., Luo, S., Wu, J., Peng, L., Cheng, F., Pan, L., Zou, J., Jia, C., Wang, Juan, Liu, X., Wang, S., Wu, X., Ge, Q., He, J., Zhan, H., Qiu, F., Guo, L., Huang, C., Jaki, T., Hayden, F.G., Horby, P.W., Zhang, D., Wang, C., 2020. A trial of lopinavir–ritonavir in adults hospitalized with severe covid-19. N. Engl. J. Med. 382, 1787–1799. https://doi.org/10.1056/nejmoa2001282.
Chen, I.-J., Foloppe, N., 2010. Drug-like bioactive structures and conformational coverage with the ligprep/confgen suite: comparison to programs MOE and catalyst. J. Chem. Inf. Model. 50, 822–839. https://doi.org/10.1021/ci100026x.
Choy, K.-T., Wong, A.Y.-L., Kaewpreedee, P., Sia, S.F., Chen, D., Hui, K.P.Y., Chu, D.K.W., Chan, M.C.W., Cheung, P.P.-H., Huang, X., Peiris, M., Yen, H.-L., 2020. Remdesivir, lopinavir, emetine, and homoharringtonine inhibit SARS-CoV-2 replication in vitro. Antivir. Res. 178, 104786 https://doi.org/10.1016/j.antiviral.2020.104786.
Chu, D.K., Akl, E.A., Duda, S., Solo, K., Yaacoub, S., Schünemann, H.J., El-harakeh, A., Bognanni, A., Lotfi, T., Loeb, M., Hajizadeh, A., Bak, A., Izcovich, A., Cuello-Garcia, C.A., Chen, C., Harris, D.J., Borowiack, E., Chamseddine, F., Schünemann, F., Morgano, G.P., Muti Schünemann, G.E.U., Chen, G., Zhao, H., Neumann, I., Chan, J., Khabsa, J., Hneiny, L., Harrison, L., Smith, M., Rizk, N., Giorgi Rossi, P., AbiHanna, P., El-khoury, R., Stalteri, R., Baldeh, T., Piggott, T., Zhang, Y., Saad, Z., Khamis, A., Reinap, M., 2020. Physical distancing, face masks, and eye protection to prevent person-to-person transmission of SARS-CoV-2 and COVID-19: a systematic review and meta-analysis. Lancet 395, 1973–1987. https://doi.org/10.1016/S0140-6736(20)31142-9.
Cooper, A.J., Scott, M.F., Rollnick, S.A., 2008. Diagnosis and treatment of infectious pharyngeal inflammation. Vestn. Otorinolaringol. 5, 57–58.
Coperchini, F., Chiovato, L., Croce, L., Magri, F., Rotondi, M., 2020. The cytokine storm in COVID-19: an overview of the involvement of the chemokine/chemokine-receptor system. Cytokine Growth Factor Rev. 53, 25–32. https://doi.org/10.1016/j.cytogfr.2020.05.003.
Damm-Ganamet, K.L., Arora, N., Becart, S., Edwards, J.P., Lebsack, A.D., McAllister, H.M., Nelen, M.I., Rao, N.L., Westover, L., Wiener, J.J.M., Mirzadegan, T., 2019. Accelerating lead identification by high Throughput virtual screening: prospective case studies from the pharmaceutical industry. J. Chem. Inf. Model. 59, 2046–2062. https://doi.org/10.1021/acs.jcim.8b00941.

Deshpande, R.R., Tiwari, A.P., Nyayanit, N., Modak, M., 2020. In silico molecular docking analysis for repurposing therapeutics against multiple proteins from SARS-CoV-2. Eur. J. Pharmacol. 886, 173430 https://doi.org/10.1016/j.ejphar.2020.173430.

Frediansyah, A., Tiwari, R., Sharun, K., Dhama, K., Harapan, H., 2020. Antivirals for COVID-19: a critical review. Clin. Epidemiol. Glob. Heal. 9, 90–98. https://doi.org/10.1016/j.cegh.2020.07.006.

Friesner, R.A., Banks, J.L., Murphy, R.B., Halgren, T.A., Klicic, J.J., Mainz, D.T., Repasky, M.P., Knoll, E.H., Shelley, M., Perry, J.K., Shaw, D.E., Francis, P., Shenkin, P.S., 2004. Glide: a New approach for rapid, accurate docking and scoring. 1. Method and assessment of docking accuracy. J. Med. Chem. 47, 1739–1749. https://doi.org/10.1021/jm0306430.

Hoffmann, M., Kleine-Weber, H., Schroeder, S., Krüger, N., Herrler, T., Erichsen, S., Schiergens, T.S., Herrler, G., Wu, N.-H., Nitsche, A., Müller, M.A., Drosten, C., Pöhlmann, S., 2020. SARS-CoV-2 cell entry depends on ACE2 and TMPRSS2 and is blocked by a clinically proven protease inhibitor. Cell 181, 271–280. https://doi.org/10.1016/j.cell.2020.02.052 e8.

Hou, Y., Zhao, J., Martin, W., Kallianpur, A., Chung, M.K., Jehi, L., Sharifi, N., Erzurum, S., Eng, C., Cheng, F., 2020. New insights into genetic susceptibility of COVID-19: an ACE2 and TMPRSS2 polymorphism analysis. BMC Med. 18 https://doi.org/10.1186/s12916-020-01673-z.

Hung, I.F.-N., Lung, K.-C., Tso, E.Y.-K., Liu, R., Chung, T.W.-H., Chu, M.-Y., Ng, Y.-Y., Lo, J., Chan, J., Tam, A.R., Shum, H.-P., Chan, V., Wu, A.K.-L., Sin, K.-M., Leung, W.-S., Law, W.-L., Lung, D.C., Sin, S., Yeung, P., Yip, C.C.-Y., Zhang, R.R., Fung, A.Y.-F., Yan, E.Y.-W., Leung, K.-H., Ip, J.D., Chu, A.W.-H., Chan, W.-M., Ng, A.C.-K., Lee, R., Fung, K., Yeung, A., Wu, T.-C., Chan, J.W.-M., Yan, W.-W., Chan, W.-M., Chan, J.F.-W., Lie, A.K.-W., Tsang, O.T.-Y., Cheng, V.C.-C., Que, T.-L., Lau, C.-S., Chan, K.-H., To, K.K.-W., Yuen, K.-Y., 2020. Triple combination of interferon beta-1b, lopinavir–ritonavir, and ribavirin in the treatment of patients admitted to hospital with COVID-19: an open-label, randomised, phase 2 trial. Lancet 395, 1695–1704. https://doi.org/10.1016/S0140-6736(20)31042-4.

Jacobson, M.P., Pincus, D.L., Rapp, C.S., Day, T.J.F., Honig, B., Shaw, D.E., Friesner, R.A., 2004. A hierarchical approach to all-atom protein loop prediction. Proteins Struct. Funct. Genet. 55, 351–367. https://doi.org/10.1002/prot.10613.

Jiang, S., Hillyer, C., Du, L., 2020. Neutralizing antibodies against SARS-CoV-2 and other human coronaviruses. Trends Immunol. 41, 355–359. https://doi.org/10.1016/j.it.2020.03.007.

Kang, C.K., Seong, M.-W., Choi, S.-J., Kim, T.S., Choe, P.G., Song, S.H., Kim, N.-J., Park, W.B., Oh, M.-D., 2020. In vitro activity of lopinavir/ritonavir and hydroxychloroquine against severe acute respiratory syndrome coronavirus 2 at concentrations achievable by usual doses. Korean J. Intern. Med. (Engl. Ed.) 35, 782–787. https://doi.org/10.3904/kjim.2020.157.

Lee, J.H., Lee, C.S., 2016. Clinical usefulness of arbekacin. Infect. Chemother. 48, 1–11. https://doi.org/10.3947/ic.2016.48.1.1.

Lotrionte, M., Biondi-Zoccai, G., Abbate, A., Lanzetta, G., D'Ascenzo, F., Malavasi, V., Peruzzi, M., Frati, G., Palazzoni, G., 2013. Review and meta-analysis of incidence and clinical predictors of anthracycline cardiotoxicity. Am. J. Cardiol. 112, 1980–1984. https://doi.org/10.1016/j.amjcard.2013.08.026.

Lovato, A., de Filippis, C., 2020. Clinical presentation of COVID-19: a systematic review focusing on upper airway symptoms. Ear Nose Throat J. 99 (9), 569–576. https://doi.org/10.1177/0145561320920762.

Lu, C.-C., Chen, M.-Y., Lee, W.-S., Chang, Y.-L., 2020. Potential therapeutic agents against COVID-19: what we know so far. J. Chin. Med. Assoc. 83, 534–536. https://doi.org/10.1097/JCMA.0000000000000318.

Madhavi Sastry, G., Adzhigirey, M., Day, T., Annabhimoju, R., Sherman, W., 2013. Protein and ligand preparation: parameters, protocols, and influence on virtual screening enrichments. J. Comput. Aided Mol. Des. 27, 221–234. https://doi.org/10.1007/s10822-013-9644-8.

Mendling, W., Weissenbacher, E.R., Gerber, S., Prasauskas, V., Grob, P., 2016. Use of locally delivered dequalinium chloride in the treatment of vaginal infections: a review. Arch. Gynecol. Obstet. 293, 469–484. https://doi.org/10.1007/s00404-015-3914-8.

Olsson, M.H.M., SØndergaard, C.R., Rostkowski, M., Jensen, J.H., 2011. PROPKA3: consistent treatment of internal and surface residues in empirical p K a predictions. J. Chem. Theory. Comput. 7, 525–537. https://doi.org/10.1021/ct100578z.

Park, J.K., Fischer, R., Dechend, R., Shagdarsuren, E., Gapeljuk, A., Wellner, M., Meiners, S., Gratze, P., Al-Saadi, N., Feldt, S., Fiebeler, A., Madwed, J.B.,

Schirdewan, A., Haller, H., Luft, F.C., Muller, D.N., 2007. p38 mitogen-activated protein kinase inhibition ameliorates angiotensin II-induced target organ damage. Hypertension 49, 481–489. https://doi.org/10.1161/01.HYP.0000256831.33459.ea.

Ramachandran, G.N., Ramakrishnan, C., Sasisekharan, V., 1963. Stereochemistry of polypeptide chain configurations. J. Mol. Biol. 7, 95–99. https://doi.org/10.1016/S0022-2836(63)80023-6.

Roos, K., Wu, C., Damm, W., Reboul, M., Stevenson, J.M., Lu, C., Dahlgren, M.K., Mondal, S., Chen, W., Wang, L., Abel, R., Friesner, R.A., Harder, E.D., 2019. OPLS3e: extending Force Field Coverage for Drug-Like Small Molecules. J. Chem. Theor. Comput. 15, 1863–1874. https://doi.org/10.1021/acs.jctc.8b01026.

Rostkowski, M., Olsson, M.H., SØndergaard, C.R., Jensen, J.H., 2011. Graphical analysis of pH-dependent properties of proteins predicted using PROPKA. BMC Struct. Biol. 11, 6 https://doi.org/10.1186/1472-6807-11-6.

Sanders, J.M., Monogue, M.L., Jodlowski, T.Z., Cutrell, J.B., 2020. Pharmacologic treatments for coronavirus disease 2019 (COVID-19): a review. JAMA, J. Am. Med. Assoc. 323, 1824–1836. https://doi.org/10.1001/jama.2020.6019.

Shelley, J.C., Cholleti, A., Frye, L.L., Greenwood, J.R., Timlin, M.R., Uchimaya, M., 2007. Epik: a software program for pKa prediction and protonation state generation for drug-like molecules. J. Comput. Aided Mol. Des. 21, 681–691. https://doi.org/10.1007/s10822-007-9133-z.

Simões E Silva, A.C., Silveira, K.D., Ferreira, A.J., Teixeira, M.M., 2013. ACE2, angiotensin-(1-7) and Mas receptor axis in inflammation and fibrosis. Br. J. Pharmacol. 169, 477–492. https://doi.org/10.1111/bph.12159.

Steffen, R., Jori, J., Dupont, H.L., Mathewson, J.J., Stürchler, D., 1993. Treatment of travellers' diarrhoea with fleroxacin: a case study. J. Antimicrob. Chemother. 31, 767–776. https://doi.org/10.1093/jac/31.5.767.

Vyas, V.K., Ukawala, R.D., Ghate, M., Chintha, C., 2012. Homology modeling a fast tool for drug discovery: current perspectives. Indian J. Pharmaceut. Sci. 74, 1–17. https://doi.org/10.4103/0250-474X.102537.

Walls, A.C., Park, Y.-J., Tortorici, M.A., Wall, A., McGuire, A.T., Veesler, D., 2020. Structure, function, and antigenicity of the SARS-CoV-2 spike glycoprotein. Cell 181, 281–292. https://doi.org/10.1016/j.cell.2020.02.058 e6.

Wang, J., 2020. Fast identification of possible drug treatment of coronavirus disease-19 (COVID-19) through computational drug repurposing study. J. Chem. Inf. Model. 60, 3277–3286. https://doi.org/10.1021/acs.jcim.0c00179.

Wrapp, D., Wang, N., Corbett, K.S., Goldsmith, J.A., Hsieh, C.-L., Abiona, O., Graham, B.S., McLellan, J.S., 2020. Cryo-EM structure of the 2019-nCoV spike in the prefusion conformation. Science 367, 1260–1263. https://doi.org/10.1126/science.aax0902, 80–.

Xu, L.-L., Zhou, X.-Q., Yi, P.-S., Zhang, M., Li, J., Xu, M.-Q., 2016. Alvimopan combined with enhanced recovery strategy for managing postoperative ileus after open abdominal surgery: a systematic review and meta-analysis. J. Surg. Res. 203, 211–221. https://doi.org/10.1016/j.jss.2016.01.027.

Ye, Z.-W., Yuan, S., Yuen, K.-S., Fung, S.-Y., Chan, C.-P., Jin, D.-Y., 2020. Zoonotic origins of human coronaviruses. Int. J. Biol. Sci. 16, 1686–1697. https://doi.org/10.7150/ijbs.45472.

Yu, X., Cui, L., Hou, F., Liu, X., Wang, Y., Wen, Y., Chi, C., Li, C., Liu, R., Yin, C., 2018. Angiotensin-converting enzyme 2-angiotensin (1-7)-Mas axis prevents pancreatic acinar cell inflammatory response via inhibition of the p38 mitogen-activated protein kinase/nuclear factor-?B pathway. Int. J. Mol. Med. 41, 409–420. https://doi.org/10.3892/ijmm.2017.3252.

Zeitlinger, M., Koch, B.C.P., Bruggemann, R., De Cock, P., Felton, T., Hites, M., Le, J., Luque, S., MacGowan, A.P., Marriott, D.J.E., Muller, A.E., Nadrah, K., Paterson, D.L., Standing, J.F., Telles, J.P., Wölfl-Duchek, M., Thy, M., Roberts, J.A., PK/PD of Anti-Infectives Study Group (EPASG) of the European Society of Clinical Microbiology, Infectious Diseases (ESCMID), 2020. Pharmacokinetics/pharmacodynamics of antiviral agents used to treat SARS-CoV-2 and their potential interaction with drugs and other supportive measures: a comprehensive review by the PK/PD of anti-infectives study group of the European society of antimicrobial agents. Clin. Pharmacokinet. 59 (10), 1195–1216. https://doi.org/10.1007/s40262-020-00924-9.

Zipeto, D., Palmeira, J.D.F., Argañaraz, G.A., Argañaraz, E.R., 2020. ACE2/ADAM17/TMPRSS2 interplay may Be the main risk factor for COVID-19. Front. Immunol. 11, 576745 https://doi.org/10.3389/fimmu.2020.576745.